Check for updates

How to cite: *Angew. Chem. Int. Ed.* **2025**, *64*, e202421942
doi.org/10.1002/anie.202421942

VIP **MOF Synthesis** **Very Important Paper**

Scalable and Low-Energy Synthesis of Metal–Organic Frameworks by a Seed-Mediated Approach

*Wentao Han, Minghao Shi, and Hai-Long Jiang**

Abstract: The synthesis of metal–organic frameworks (MOFs) by low energy input has been a long-term target for practical applications yet remains a great challenge. Herein, we developed a low-energy MOF growth strategy at a temperature down to 50 °C by simply introducing seeds into the reaction system. The MOFs are continuously grown on the surface of the seeds at a growth rate dozens of times higher than that of conventional solvothermal synthesis at low temperature, while the resulting MOFs possess high crystallinity, porosity, and stability similar to solvothermal seeds. Remarkably, the obtained MOFs feature high-density structural defects with Lewis acidity, thereby displaying more than one order of magnitude higher activity than the MOFs obtained by the conventional solvothermal method in the iodination reaction of substituted arenes. This low-energy synthetic approach is readily scaled up, which would be a significant step forward in the dream of the MOF industry.

Introduction

Metal–organic frameworks (MOFs), as a class of crystalline porous materials with excellent crystallinity, porosity, and designability, have attracted great attention since their appearance.[1] They have been recognized to be very promising in diverse fields, such as sorption and separation, catalysis, optics, proton conductivity, drug delivery, and others, in recent years.[2] The development of a synthetic methodology provides a solid foundation for the structural diversity and applications of MOFs. Among diverse synthetic approaches, the conventional solvothermal method is the most widely adopted for MOF synthesis. Unfortunately, it usually requires a relatively high temperature and long reaction time and may generate hazardous autogenous pressure, thereby not coming up with the demands of green chemistry and future industry. To meet the requirements of the MOF industry, the development of a new synthetic strategy that is amenable to the concept of "green synthesis" by a simple operation under mild conditions, especially at low temperatures, has been a long-term yet challenging goal.

Among a variety of MOFs, Zr-based MOFs have been intensively studied and exhibit broad applications due to their high stability.[3] Unfortunately, relatively high reaction temperatures (usually $\geq$120 °C) are adopted in the synthesis of Zr-based MOFs because of the high energy for the formation of reversible yet strong Zr–O coordination bonds. In previous studies, there are two common routes to synthesize Zr-carboxylate MOFs at low temperatures. One is to reduce the energy of nucleation and growth by adding auxiliary agents, such as anions, acid/base regulators, and ionic liquids,[4] which brings in waste and significantly changes the synthetic recipe for MOFs in addition to the reaction temperature, making it difficult in universality. The other way is to supply energy in other forms rather than by simply heating, such as spray-drying, mechanochemical, and electrochemical methods,[5] to increase the reaction rate and/or reduce the synthetic temperature. These methods present shortcomings to a certain degree. Therefore, the development of a truly low-energy strategy to synthesize Zr-based MOFs with high crystallinity and quantity in a simple way remains highly desired.

According to classical nucleation theory and the reported growth mechanism for MOFs,[6] MOF growth generally experiences nucleation and subsequent growth stages, in which the energy barrier associated with the nucleation process is difficult to surmount at low reaction temperatures. Inspired by the heterogeneous nucleation in traditional crystallography and seed-induced zeolite synthesis,[7] we have previously achieved the synthesis of phase pure MOFs by a seed-mediated strategy during solvothermal growth,[8] preliminarily demonstrating the feasibility of promoting MOF growth by pre-introducing crystal seeds. Despite the great potential of the seed-mediated strategy, how the MOF growth process is influenced by the introduced seeds and whether the reactants are grown on the seeds or homogeneously nucleate to grow up remains unknown.

Herein, the introduction of crystal seeds leads to the successful synthesis of diverse Zr-based MOFs at a much lower temperature than that in their typical solvothermal synthesis (Scheme 1). The seeds of the four representative types of Zr-based MOFs, denoted as **UiO-66$_{seed}$**, **UiO-66-NH$_{2seed}$**, **MOF-808$_{seed}$**, and **DUT-67$_{seed}$**, are obtained by solvothermal conditions at 100–120 °C. By incorporating these seeds into their respective reaction systems, the corresponding MOFs with crystallinity and porosity comparable to those of the seeds are successfully obtained at a reaction temperature as low as 50 °C and even room temperature. It is found that the MOFs experience epitaxial growth on the surface of

[*] W. Han, M. Shi, Prof. Dr. H.-L. Jiang
Hefei National Research Center for Physical Sciences at the Microscale, Department of Chemistry, University of Science and Technology of China, Hefei, Anhui 230026 (P. R. China)
E-mail: jianglab@ustc.edu.cn
Homepage: http://mof.ustc.edu.cn/

© 2025 Wiley-VCH GmbH

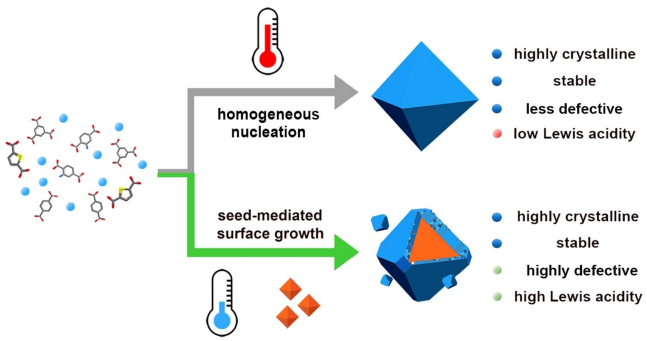

Scheme 1. illustration showing low-energy MOF growth on crystal seeds. Compared to the traditionally synthesized MOF seeds at higher temperatures, the seed-mediated method generates MOF particles with evolutionary morphology and abundant defects and high Lewis acidity at low temperatures.

the seed crystals at low temperature. This surface growth was unambiguously confirmed by strategically constructing a Hf@Zr core–shell structure whose compositional distribution was directly visualized by scanning transmission electron microscopy (STEM) image and energy-dispersive X-ray spectroscopy (EDS) line scanning. Prominent morphology evolution is accompanied by surface growth, to which both thermodynamic and kinetic factors are believed to contribute. Furthermore, abundant defects are generated in the seed-mediated MOFs synthesized at low temperature, giving rise to their much-enhanced Lewis acidity. As a result, these MOFs exhibit several times higher activity than those of seed crystals made by a high-temperature solvothermal method in the C–H iodination reaction of aromatic hydrocarbons. In addition, the one-pot, 5-gram-scale synthesis of **MOF-808** as a representative has been achieved at 50 °C, manifesting the great opportunity of such a synthetic strategy for large-scale MOF preparation for future applications.

Results and Discussion

During the preliminary experiments, MOFs involving various metals have been examined (Figure S1), and results indicate that Zr-based MOFs are highly compatible with the seed-mediated method. The 6-connected Zr-MOF, **MOF-808**, is selected for the demonstration of seed-asisted growth at low temperature, as its regular shape is favorable for the observation of its morphology evolution. The seed crystals of **MOF-808**, denoted **MOF-808$_{seed}$**, are obtained under the reported solvothermal conditions by reacting $ZrOCl_2 \cdot 8H_2O$ and benzene-1,3,5-tricarboxylic acid in a mixture of *N,N*-dimethylformamide and formic acid at 100 °C.[9] The obtained seed crystals are then added to the reaction with the same reactant concentration as that in the above solvothermal condition. The products from the seed-mediated conditions are collected after different reaction time lengths at specific temperatures. Although MOF growth is slow at 25 °C, 41.3 mg of product can be obtained after 30 days of standing (Table S1). To our delight, 54 mg of **MOF-808** was produced in only one day at 50 °C under continuous stirring (Table S2). In contrast, the system without seed crystals fails to give any product at either temperature. When the reaction temperature increases to 75 °C, the **MOF-808** yield with or without the addition of the seed crystals becomes comparable (Figure S2). It is thus obvious that although the self-nucleation of **MOF-808** is difficult at low temperatures, the addition of seed crystals efficiently promotes the formation of products.

Powder X-ray diffraction (XRD) patterns support that the seed-mediated **MOF-808** synthesized at 50 °C (default otherwise stated for **MOF-808**) and even room temperature possesses similar high crystallinity to the parent seeds (Figures 1a and S3). N_2 sorption isotherms at 77 K reveal a highly porous structure of **MOF-808** with Brunauer–Emmett–Teller (BET) surface area of 1081 $m^2 g^{-1}$, which is 162 % of that for **MOF-808$_{seed}$** (669 $m^2 g^{-1}$; Figure 1b). These results demonstrate that **MOF-808** synthesized using the seed-mediated method at low temperature has excellent crystallinity and high porosity, which are even higher than those under traditional solvothermal conditions. Scanning electron microscopy (SEM) images show that **MOF-808** has a cuboctahedron morphology with sizes larger than the seeds (Figures 1c, d and S4).

Furthermore, the seed-mediated low-energy method can be extended to the synthesis of other commonly used Zr-based MOFs, including **UiO-66**, **UiO-66-NH$_2$**, and **DUT-67**,[10] at low temperatures (Figure S5), yielding the corresponding products with high crystallinity, regular morphology, and expected surface areas (Figures S6–11). The above results reflect that seed-mediated low-energy growth at low temperatures is generally applicable to the synthesis of different Zr-based MOFs and possibly extendable to more diverse compounds.

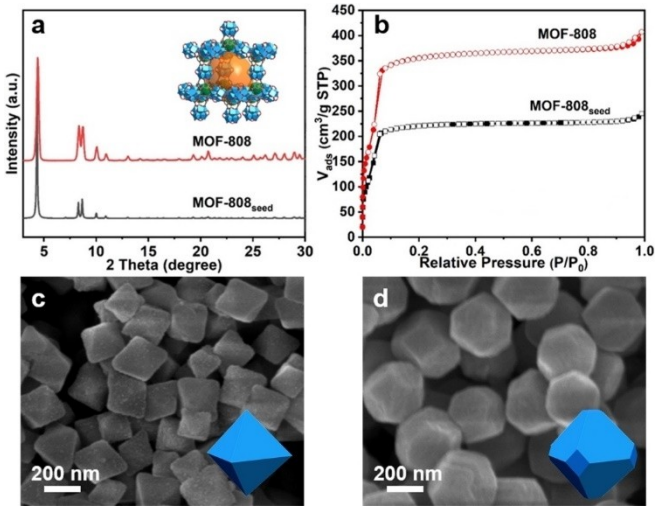

Figure 1. Comparison of MOF-808$_{seed}$ and the seed-mediated synthesized MOF-808. a) Powder XRD patterns of MOF-808$_{seed}$ and MOF-808 (inset: the partial structure of MOF-808 with highlighted pores. b) N_2 sorption isotherms for MOF-808$_{seed}$ and MOF-808 at 77 K. c) and d) SEM images of c) MOF-808$_{seed}$ and d) MOF-808 (insets: ideal morphology).

© 2025 Wiley-VCH GmbH

15213773, 2025, 13, Downloaded from https://onlinelibrary.wiley.com/doi/10.1002/anie.202421942 by University Of Science, Wiley Online Library on [27/03/2025]. See the Terms and Conditions (https://onlinelibrary.wiley.com/terms-and-conditions) on Wiley Online Library for rules of use; OA articles are governed by the applicable Creative Commons License

To further understand the growth mechanism, classical nucleation theory (CNT) is used to explain the growth process. According to CNT, the nucleation and growth of MOFs are strongly associated with the concentration of the building blocks and energy input (Figure 2a).[6] During the synthetic steps, the nucleation process (red part) would be inhibited by the high surface energy of the crystal nucleus under relatively low concentration and low-energy input conditions, which should be the main obstacle to the low-temperature synthesis of MOFs. In contrast, the growth of MOFs (blue part) can be carried out under low-energy conditions, during which the nucleation rate is close to zero. Given the above successful synthesis of different MOFs at low temperatures by adding seeds, it is assumed that the MOFs in our case might heterogeneously nucleate and grow on the seeds and bypass the high-energy self-nucleation step.

To experimentally validate the above assumption, the surface growth is initially monitored by electron microscopy. The original octahedral shape of **UiO-66**, **MOF-808**$_{seed}$ and **UiO-66-NH**$_{2seed}$ and the truncated cube morphology of **DUT-67** are transformed to cuboctahedron for all their corresponding MOFs at low temperature (Figures 1d, 2b and S7). Considering that the relatively strong Zr–O coordination bonds in Zr-based MOFs will likely rule out the possibility of the restructuring process, which may cause morphological changes in the low-temperature reaction (Figure S12), the formation of the observed new morphology should be a result of surface growth during the seed-mediated synthetic process. Such great changes in morphology may be attributed to the combination of both the thermodynamic and kinetic factors.[11] Firstly, compared with common octahedral and cubic morphology, which have (111) and (100) planes exclusively exposed, respectively, the cuboctahedral morphology has a mix of (111) and (100) planes. The nearly spherical geometry of the cuboctahedral morphology can minimize the facet area to achieve the minimum interfacial free energy (Figure 2b).[12] Secondly, the surface growth of MOFs is often related to the formation of secondary building units (SBUs) and the attachment of SBUs to the surface of MOF crystallites.[6b–d] When MOFs are synthesized at low temperatures, the attachment of SBU to exposed facets will be different from that at high temperatures, resulting in different growth rates of exposed facets. Since the crystal facet that grows at the slowest rate will be exposed on the surface, the altered growth kinetics of facets at low temperature might also cause the evolution of morphologies.

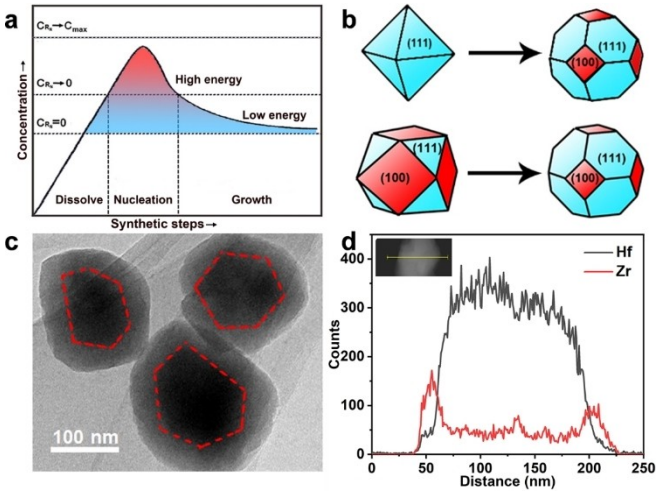

Figure 2. Seed-mediated surface growth. a) Schematic illustration showing the change in precursor concentration during synthetic steps, which is similar to LaMer's model. The nucleation process is marked in red to reflect its higher energy requirement. b) Morphological changes of MOFs during seed-mediated synthesis. MOF-808 and UiO-66-NH_2 change from octahedron to cuboctahedron (top), and DUT-67 changes from truncated cube to cuboctahedron (bottom). c) Transmission electron microscopy (TEM) image of UiO-66(Hf)@UiO-66(Zr). The dark core in each particle is outlined with red dashed lines. d) The EDS line-scan profile through the particles of UiO-66(Hf)@UiO-66(Zr). The STEM image shows the selection area along the yellow line (inset).

To provide visual evidence for the growth process of the size and weight of **MOF-808** crystallites over time, small-sized grains of **MOF-808**$_{seed}$ were used as seeds for the low-temperature synthesis, during which the concentration of the solution was controlled by continuous feeding. During growth, the size of **MOF-808** remained uniform without the formation of small particles (Figure S13). The identical crystal size and regular morphology suggest that **MOF-808** tends to grow on the seed surface rather than self-nucleate. The weight of the obtained MOF exhibits a cubic polynomial relationship with the reaction time, implying that the MOF growth rate increases with the total surface area exposed of the MOF in the system (Figure S14). More direct evidence for MOF growth on the surface has been obtained by establishing a growth layer that is different from the original seed in its composition. **UiO-66(Hf)** is used as the seed for the epitaxial growth of **UiO-66(Zr)**, which affords a core–shell structure of **UiO-66(Hf)@UiO-66(Zr)**. TEM image exhibits the darker inner Hf core and the brighter outer Zr layer in each particle of **UiO-66(Hf)@UiO-66(Zr)**. Meanwhile, the EDS line scanning further confirms the core–shell distribution of Hf and Zr elements in the particle (Figure 2c, d). The above results provide strong evidence of the surface growth of seed crystals.

In addition, with the addition of larger-size seeds whose surface is closer to an infinite two-dimensional plane, island-like nuclei growth occurs on the seed surface.[13] SEM images show that different sizes of **MOF-808**$_{seed}$ led to different growth pathways (Figure S15). Small-size seeds give rise to epitaxial growth, while large-size seeds produce island-like nuclei on the surface.[13] These nuclei readily fall off due to vigorous stirring prior to the formation of the growth layer, which explains the generation of crystallites when large-size seeds are used (Figure S7e, f). Since self-nucleation does not occur in the solution without seeds, we believe that these small-size crystals are all produced via island-like nuclei growth on the seed crystals (Table S3).

In MOF synthesis at high temperatures, the thermodynamically controlled reversible formation of coordination bonds between the metal and linker will promote the growth of relatively perfect crystals. In contrast, during synthesis at low temperatures, MOF growth tends to be a kinetic process. The crystal structure will expand before the precursor can

© 2025 Wiley-VCH GmbH

15213773, 2025, 13, Downloaded from https://onlinelibrary.wiley.com/doi/10.1002/anie.202421942 by University Of Science, Wiley Online Library on [27/03/2025]. See the Terms and Conditions (https://onlinelibrary.wiley.com/terms-and-conditions) on Wiley Online Library for rules of use; OA articles are governed by the applicable Creative Commons License

repair the coordination vacancy in the lattice to result in unique structural characteristics, such as enlarged pore sizes and more defects compared with those in MOFs obtained at high temperatures.[14] In particular, defect-associated open metal sites with strong Lewis acidity can serve as adsorption and activation sites for substrates, which will endow the seed-mediated MOFs with unique advantages in catalytic reactions. Besides defects, the generation of mesopores from coordination vacancies would also be favorable for catalysis.[15]

To probe and analyse these features of the seed-mediated MOFs at low temperatures, characterizations with various techniques have proceeded. Powder XRD patterns of **UiO-66-NH$_2$** show two new diffraction peaks at 4° and 6° (Figure S6), which correspond to the (100) and (110) diffraction planes, respectively. The anomalies of structural extinction represent a transition of topology from **fcu** to **reo**, which is an important sign of cluster defects.[16] In addition, the rapidly increased N_2 adsorption in the p/p_0 range of 0.4–0.7 and the expanded pore size distribution for seed-mediated **UiO-66** demonstrate that there are a large number of mesopores produced at low temperatures (Figure S9), which implies the presence of linker and metal-oxo cluster vacancies. Thermogravimetric (TG) curves reveal that the organic linker-associated weight loss is reduced in seed-mediated MOFs compared to their corresponding seeds (Figure S16). The number of BDC is determined by the quality loss after 500 °C according to the existing scheme and further compared with reported defective **UiO-66** (Table S4).[4c,17] In addition, ^{1}H nuclear magnetic resonance (NMR) spectra show a reduced amount of formic acid relative to the linker in seed-mediated MOFs (Figures S17–S20). To calculate the defect content, Zr, ligand, and formic acid were quantified by inductively coupled plasma atomic emission spectroscopy (ICP-AES) and NMR, and the molar ratio of the structure was obtained (Table S5). Considering that formic acid acts as a difficult-to-remove capping agent bond to the open sites of Zr-oxo clusters, the disappeared formic acid will be replaced by some easily leaving ligands, such as OH^-, H_2O or Cl^-, which facilitates the activation of the Zr(IV) sites. The above analyses reflect the unique merits of structural defects in MOFs synthesized by the seed-mediated method, which lays the foundation for their applications that might be beyond the capability of solvothermal seeds. Due to the presence of linker and metal-oxo cluster vacancies, more Lewis acid sites and mesopores exist in the seed-mediated MOFs, which is beneficial to their applications in catalysis.[18]

Strikingly, upon sufficient activation, the seed-mediated **MOF-808** gives the product of 1-iodo-2-methoxynaphthalene in a yield of 92.5 %, while the corresponding yield by **MOF-808$_{seed}$** is only 5.1 % in the C–H iodination of 2-methoxynaphthalene in 24 hours at room temperature. Such a stark difference in activity is also reflected in the comparison between **UiO-66**, **UiO-66-NH$_2$** and their respective seeds (Figure 3b). The yields of iodinated products after a one-day reaction at room temperature are 2.0 % and 4.8 % by **UiO-66$_{seed}$** and **UiO-66-NH$_{2seed}$**, respectively, which are significantly improved to 98.5 % and 99 %, respectively, by using seed-mediated **UiO-66** and **UiO-66-NH$_2$**. **MOF-808** maintains its

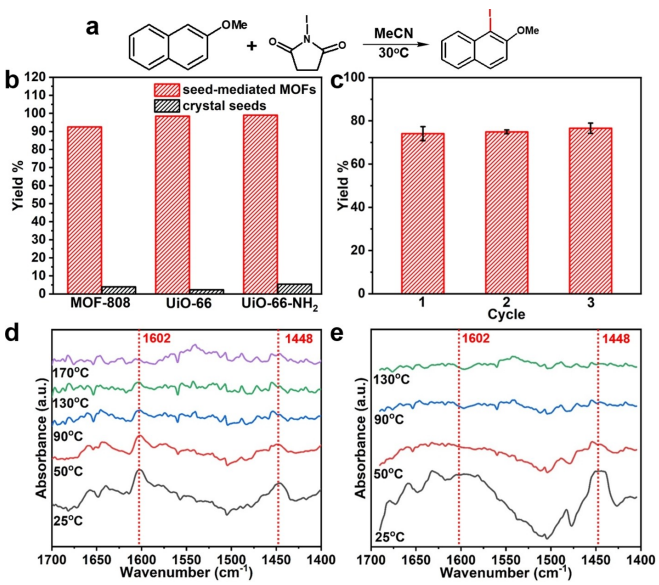

Figure 3. a) Catalytic C–H iodination reaction of 2-methoxynaphthalene. b) The yield of 1-iodo-2-methoxynaphthalene after 24 hours of reaction at room temperature by using different catalysts. c) Three catalytic cycles of MOF-808 with each cycle of 4 hours. The cyclic experiment was conducted in three parallel trials to ensure reproducibility. In situ DRIFTS spectra of pyridine adsorption on d) MOF-808 and e) MOF-808$_{seed}$. The two characteristic peaks of Lewis acid at 1602 cm^{-1} and 1448 cm^{-1} are marked by red dotted lines.

activity in three consecutive runs of C–H iodination (Figure 3c), indicating its good recyclability, which may be ascribed to its stable Zr-linker skeleton and robust defect sites. To further generate the active sites, we treat **UiO-66$_{seed}$** and **UiO-66-NH$_{2seed}$** with HCl, during which the potential Lewis acid sites occupied by the HCOOH modulator on the Zr-oxo clusters are released out and exposed (Figure S21a, b).[20] As a result, high activities are obtained (Figure S21d), reflecting the importance of generating Lewis acid sites by HCl treatment for catalysis. By contrast, the seed-mediated MOF can be fully activated by simple thermal activation only.

The more than one order of magnitude improvements in catalytic activity should be ascribed to the much stronger Lewis acidity in seed-mediated MOFs than that in the MOF seeds. To examine their difference in Lewis acidity, in situ diffuse reflectance infrared Fourier transform spectroscopy (DRIFTS) spectra of pyridine adsorbed on **MOF-808** were collected at different temperatures (Figure 3d, e). The spectrum at 298 K on seed-mediated **MOF-808** possesses characteristic absorption peaks of pyridine at 1448 cm^{-1} and 1602 cm^{-1}, corresponding to the adsorption of pyridine on Lewis acid sites that are associated with defects on Zr_6 clusters.[21] At higher temperatures, the characteristic peaks gradually weaken and disappear at 170 °C. In contrast, when pyridine is adsorbed on **MOF-808$_{seed}$**, only one band at 1448 cm^{-1} can be observed, which drops rapidly when the temperature is raised to 50 °C only, indicating a much weaker interaction between the Zr-oxo cluster and pyridine. Therefore, it is evident that seed-mediated **MOF-808** possesses a much stronger Lewis acidity than its corresponding seed.

© 2025 Wiley-VCH GmbH

15213773, 2025, 13, Downloaded from https://onlinelibrary.wiley.com/doi/10.1002/anie.202421942 by University Of Science, Wiley Online Library on [27/03/2025]. See the Terms and Conditions (https://onlinelibrary.wiley.com/terms-and-conditions) on Wiley Online Library for rules of use; OA articles are governed by the applicable Creative Commons License

Defects have long been considered to be detrimental to physicochemical properties, as they may result in poor stability.[22] Interestingly, in our case, we find that these MOFs maintain a high level of thermal and acid-base stability even with a large number of defects. As shown by TG curves, although the presence of linker and metal-oxo cluster vacancies results in decreased weight losses, the temperatures corresponding to each weight loss step do not change (Figure S16), which suggests the undisturbed thermal stability of seed-mediated MOFs to their parent seeds. In addition, seed-mediated MOFs immersed in aqueous acidic and alkaline solutions at different pH values for 24 hours exhibit similar powder XRD patterns to those of untreated MOFs, indicating their good chemical stability (Figure S22). The good thermal and chemical stability found in the seed-mediated MOFs demonstrates that the robust Zr–O bonds may dominate the stability of the frameworks, which minimizes the possible detrimental influence caused by the presence of defects.

With the great potential in diverse applications, MOFs have long been expected to be commercialized.[23] However, the extensive industrial use of MOFs is still limited by their energy-intensive and hazardous large-scale production where high temperature and autogenous pressure are involved. Hence, the large-scale production of high-performance MOFs under benign conditions is urgent yet remains challenging.[24] Our aforementioned results manifest the high catalyst activity and stability of seed-mediated MOFs, making it worth evaluating their good application prospects. Considering that the seed-mediated synthesis of MOFs can be conducted at a low temperature under continuous stirring conditions, a scaled-up synthesis was carried out (Figure 4a). The synthetic system of MOF-808 was proportionally scaled up to a 1 L vessel in our preliminary attempt. The use of 1 g of seed crystals allows the harvest of 5.6 g product (named **MOF-808$_{LS}$**, where LS means large-scale) in one-pot synthesis within one day. **MOF-808$_{LS}$** possesses high crystallinity and BET surface area (1131 $m^2 g^{-1}$) (Figure 4b, c), which demonstrates the excellent applicability of the seed-mediated method for scale-up production.

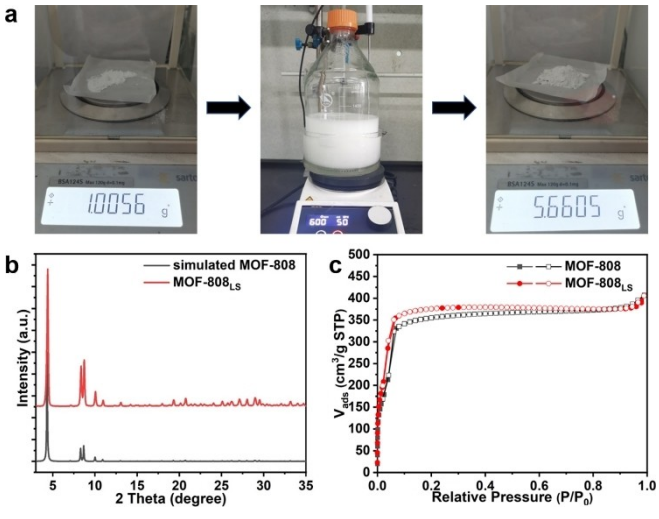

Figure 4. Scale-up synthesis of MOF-808 by seed-mediated approach. a) Photos of seed-mediated synthesis of MOF-808$_{LS}$ in a 1 L-scale vessel where 5.66 g product is obtained with 1 g crystal seeds. b) Powder XRD pattern of MOF-808$_{LS}$. c) N_2 sorption isotherms for MOF-808$_{LS}$ and MOF-808 at 77 K.

Conclusions

In summary, we have presented a seed-mediated strategy for low-energy MOF synthesis at low temperatures. By adding a small amount of pre-made MOF seeds, the precursors can be induced to grow on the external surfaces of seed crystals, yielding the corresponding MOF products efficiently at close to ambient temperature. The obtained MOFs not only possess comparable crystallinity, porosity, and stability to their seeds but also exhibit new morphology and additional mesoporosity. Remarkably, the emergent strong Lewis acidity in the seed-mediated MOFs results in ten-fold superior activity to seed MOFs in the catalytic aromatic iodination of 2-methoxynaphthalene. In addition, seed-mediated low-energy MOF synthesis can be successfully scaled up without any sacrifice of the material quality, demonstrating its promising applicability in large-scale synthesis. This work opens up an avenue for the low-energy synthesis of MOFs with engineered porosity and defect features, paving the way for large-scale MOF synthesis at low temperatures.

Acknowledgements

This work was supported by the National Key Research and Development Program of China (2021YFA1500400), the National Natural Science Foundation of China (22331009, U22A20401) and the Strategic Priority Research Program of the Chinese Academy of Sciences (XDB0450302, XDB0540000). This work was partially carried out at the Instruments Center for Physical Science, USTC.

Conflict of Interest

The authors declare the following competing financial interest(s): A China patent application on this work has been led (China Patent Number ZL202211607463.5), where H. L. J. and W. H. are listed as inventors.

Data Availability Statement

The data that support the findings of this study are available from the corresponding author upon reasonable request.

Keywords: metal–organic frameworks · Lewis acids · low-energy synthesis · seed-mediated synthesis · heterogeneous catalysis

© 2025 Wiley-VCH GmbH

15213773, 2025, 13, Downloaded from https://onlinelibrary.wiley.com/doi/10.1002/anie.202421942 by University Of Science, Wiley Online Library on [27/03/2025]. See the Terms and Conditions (https://onlinelibrary.wiley.com/terms-and-conditions) on Wiley Online Library for rules of use; OA articles are governed by the applicable Creative Commons License

[1] a) H.-C. Zhou, J. R. Long, O. M. Yaghi, *Chem. Rev.* **2012**, *112*, 673–674; b) H. Furukawa, K. E. Cordova, M. O'Keeffe, O. M. Yaghi, *Science* **2013**, *341*, 1230444; c) S. Jeoung, S. Kim, M. Kim, H. R. Moon, *Coord. Chem. Rev.* **2020**, *420*, 213377; d) L. Jiao, H.-L. Jiang, *Chin. J. Catal.* **2023**, *45*, 1–5.

[2] a) H.-C. Zhou, S. Kitagawa, *Chem. Soc. Rev.* **2014**, *43*, 5415–5418; b) B. Li, H.-M. Wen, Y. Cui, W. Zhou, G. Qian, B. Chen, *Adv. Mater.* **2016**, *28*, 8819–8860; c) D. Liu, J. Wan, G. Pang, Z. Tang, *Adv. Mater.* **2019**, *31*, 1803291; d) Q.-G. Zhai, X. Bu, X. Zhao, D.-S. Li, P. Feng, *Acc. Chem. Res.* **2017**, *50*, 407–417; e) Y. H. Wijesundara, T. S. Howlett, S. Kumari, J. J. Gassensmith, *Chem. Rev.* **2024**, *124*, 3013–3036.

[3] a) S. Daliran, A. R. Oveisi, C.-W. Kung, U. Sen, A. Dhakshinamoorthy, C.-H. Chuang, M. Khajeh, M. Erkartal, J. T. Hupp, *Chem. Soc. Rev.* **2024**, *53*, 6244–6294; b) Y. Bai, Y. Dou, L.-H. Xie, W. Rutledge, J.-R. Li, H.-C. Zhou, *Chem. Soc. Rev.* **2016**, *45*, 2327–2367.

[4] a) K. Li, J. Yang, J. Gu, *Chem. Sci.* **2019**, *10*, 5743–5748; b) Y. Li, J. Su, Y. Zhao, L. Feng, L. Gao, X. Xu, Y. Yin, Y. Liu, P. Xiao, L. Yuan, J.-S. Qin, Y. Wang, S. Yuan, H. Zheng, J.-L. Zuo, *J. Am. Chem. Soc.* **2023**, *145*, 10227–10235; c) X. Sang, J. Zhang, J. Xiang, J. Cui, L. Zheng, J. Zhang, Z. Wu, Z. Li, G. Mo, Y. Xu, J. Song, C. Liu, X. Tan, T. Luo, B. Zhang, B. Han, *Nat. Commun.* **2017**, *8*, 175.

[5] a) N. Stock, S. Biswas, *Chem. Rev.* **2012**, *112*, 933–969; b) Carné-Sánchez, I. Imaz, M. Cano-Sarabia, D. Maspoch, *Nat. Chem.* **2013**, *5*, 203–211; c) Karadeniz, D. Žilić, I. Huskić, L. S. Germann, A. M. Fidelli, S. Muratović, I. Lončarić, M. Etter, R. E. Dinnebier, D. Barišić, N. Cindro, T. Islamoglu, O. K. Farha, T. Friščić, K. Užarević, *J. Am. Chem. Soc.* **2019**, *141*, 19214–19220; d) T. J. Azbell, T. A. Pitt, R. T. Jerozal, R. M. Mandel, P. J. Milner, *Acc. Mater. Res.* **2023**, *4*, 867–878.

[6] a) V. K. LaMer, R. H. Dinegar, *J. Am. Chem. Soc.* **1950**, *72*, 4847–4854; b) M. J. Van Vleet, T. Weng, X. Li, J. R. Schmidt, *Chem. Rev.* **2018**, *118*, 3681–3721; c) J. Han, X. He, J. Liu, R. Ming, M. Lin, H. Li, X. Zhou, H. Deng, *Chem* **2022**, *8*, 1637–1657; d) B. P. Carpenter, A. R. Talosig, B. Rose, G. Di Palma, J. P. Patterson, *Chem. Soc. Rev.* **2023**, *52*, 6918–6937.

[7] a) J. Zhang, L. Wang, B. Zhang, H. Zhao, U. Kolb, Y. Zhu, L. Liu, Y. Han, G. Wang, C. Wang, D. S. Su, B. C. Gates, *Nat. Catal.* **2018**, *1*, 540–546; b) J. Mallette, S. Seo, J. D. Rimer, *Nat. Synth.* **2022**, *1*, 521–534; c) Y. Liu, X. Wang, J. Li, Q. Zhang, Z. Niu, S. Wang, Y. Gao, M. Gao, R. Bai, Y. Zhou, W. Fan, O. Terasaki, J. Xu, J. Yu, *Angew. Chem. Int. Ed.* **2023**, *62*, e202312131.

[8] H.-Q. Xu, K. Wang, M. Ding, D. Feng, H.-L. Jiang, H.-C. Zhou, *J. Am. Chem. Soc.* **2016**, *138*, 5316–5320.

[9] a) H. Furukawa, F. Gándara, Y.-B. Zhang, J. Jiang, W. L. Queen, M. R. Hudson, O. M. Yaghi, *J. Am. Chem. Soc.* **2014**, *136*, 4369–4381; b) J. Li, H. Huang, W. Xue, K. Sun, X. Song, C. Wu, L. Nie, Y. Li, C. Liu, Y. Pan, H.-L. Jiang, D. Mei, C. Zhong, *Nat. Catal.* **2021**, *4*, 719–729; c) J. Jiang, F. Gándara, Y.-B. Zhang, K. Na, O. M. Yaghi, W. G. Klemperer, *J. Am. Chem. Soc.* **2014**, *136*, 12844–12847.

[10] a) J. H. Cavka, S. Jakobsen, U. Olsbye, N. Guillou, C. Lamberti, S. Bordiga, K. P. Lillerud, *J. Am. Chem. Soc.* **2008**, *130*, 13850–13851; b) M. Kandiah, M. H. Nilsen, S. Usseglio, S. Jakobsen, U. Olsbye, M. Tilset, C. Larabi, E. A. Quadrelli, F. Bonino, K. P. Lillerud, *Chem. Mater.* **2010**, *22*, 6632–6640; c) V. Bon, I. Senkovska, I. A. Baburin, S. Kaskel, *Cryst. Growth Des.* **2013**, *13*, 1231–1237.

[11] a) S. Dai, F. Nouar, S. Zhang, A. Tissot, C. Serre, *Angew. Chem. Int. Ed.* **2021**, *60*, 4282–4288; b) X. G. Wang, Q. Cheng, Y. Yu, X. Z. Zhang, *Angew. Chem. Int. Ed.* **2018**, *57*, 7836–7840.

[12] Y. Xia, Y. Xiong, B. Lim, S. E. Skrabalak, *Angew. Chem. Int. Ed.* **2009**, *48*, 60–103.

[13] K. Y. Ma, L. Zhang, S. Jin, Y. Wang, S. I. Yoon, H. Hwang, J. Oh, D. S. Jeong, M. Wang, S. Chatterjee, G. Kim, A. R. Jang, J. Yang, H. Y. Ryu, R. S. Ruoff, M. Chhowalla, F. Ding, H. S. Shin, *Nature* **2022**, *606*, 88–93.

[14] G. C. Shearer, S. Chavan, J. Ethiraj, J. G. Vitillo, S. Svelle, U. Olsbye, C. Lamberti, S. Bordiga, K. P. Lillerud, *Chem. Mater.* **2014**, *26*, 4068–4071.

[15] a) L. Feng, G. S. Day, K.-Y. Wang, S. Yuan, H.-C. Zhou, *Chem* **2020**, *6*, 2902–2923; b) H. Xu, J. Han, B. Zhao, R. Sun, G. Zhong, G. Chen, Y. Yamauchi, B. Guan, *Nat. Commun.* **2023**, *14*, 8062.

[16] a) M. J. Cliffe, W. Wan, X. Zou, P. A. Chater, A. K. Kleppe, M. G. Tucker, H. Wilhelm, N. P. Funnell, F.-X. Coudert, A. L. Goodwin, *Nat. Commun.* **2014**, *5*, 4176; b) C. Chen, L. Meng, L. Cao, D. Zhang, S. An, L. Liu, J. Wang, G. Li, T. Pan, J. Shen, Z. Chen, Z. Shi, Z. Lai, Y. Han, *J. Am. Chem. Soc.* **2024**, *146*, 11855–11865.

[17] a) L. Valenzano, B. Civalleri, S. Chavan, S. Bordiga, M. H. Nilsen, S. Jakobsen, K. P. Lillerud, C. Lamberti, *Chem. Mater.* **2011**, *23*, 1700–1718; b) M. Abdel-Mageed, B. Rungtaweevoranit, M. Parlinska-Wojtan, X. Pei, O. M. Yaghi, R. J. Behm, *J. Am. Chem. Soc.* **2019**, *141*, 5201–5210; c) F. Vermoortele, B. Bueken, G. L. Bars, B. Van de Voorde, M. Vandichel, K. Houthoofd, A. Vimont, M. Daturi, M. Waroquier, V. Van Speybroeck, C. Kirschhock, D. E. De Vos, *J. Am. Chem. Soc.* **2013**, *135*, 11465–11468; d) M. R. DeStefano, T. Islamoglu, S. J. Garibay, J. T. Hupp, O. K. Farha, *Chem. Mater.* **2017**, *29*, 1357–1361; e) X. Feng, J. Hajek, H. S. Jena, G. Wang, S. K. P. Veerapandian, R. Morent, N. De Geyter, K. Leyssens, A. E. J. Hoffman, V. Meynen, C. Marquez, D. E. De Vos, V. Van Speybroeck, K. Leus, P. Van Der Voort, *J. Am. Chem. Soc.* **2020**, *142*, 3174–3183; f) F. Zhou, N. Lu, B. Fan, H. Wang, R. Li, *J. Energy Chem.* **2016**, *25*, 874–879.

[18] a) X. Ma, L. Wang, Q. Zhang, H.-L. Jiang, *Angew. Chem. Int. Ed.* **2019**, *58*, 12175–12179; b) S. Dai, C. Simms, G. Patriarche, M. Daturi, A. Tissot, T. N. Parac-Vogt, C. Serre, *Nat. Commun.* **2024**, *15*, 3434.

[19] a) J. M. Saya, T. R. Roose, J. J. Peek, B. Weijers, T. J. S. de Waal, C. M. L. Vande Velde, R. V. A. Orru, E. Ruijter, *Angew. Chem. Int. Ed.* **2018**, *57*, 15232–15236; b) Sakakura, A. Ukai, K. Ishihara, *Nature* **2007**, *445*, 900–903.

[20] G. Cai, H.-L. Jiang, *Angew. Chem. Int. Ed.* **2017**, *56*, 563–567.

[21] T. H. Vuong, N. Rockstroh, U. Bentrup, J. Rabeah, J. Knossalla, S. Peitz, R. Franke, A. Brückner, *ACS Catal.* **2021**, *11*, 3541–3552.

[22] G. Liu, Y. Guo, C. Chen, Y. Lu, G. Chen, G. Liu, Y. Han, W. Jin, N. Xu, *Nat. Mater.* **2023**, *22*, 769–776.

[23] M. Wright, M. T. Kapelewski, S. Marx, O. K. Farha, *Nat. Mater.* **2024**, DOI: 10.1038/s41563-024-019-4.

[24] P. Silva, S. M. Vilela, J. P. Tome, F. A. A. Paz, *Chem. Soc. Rev.* **2015**, *44*, 6774–6803.

Manuscript received: November 11, 2024
Accepted manuscript online: January 7, 2025
Version of record online: January 16, 2025

© 2025 Wiley-VCH GmbH

15213773, 2025, 13, Downloaded from https://onlinelibrary.wiley.com/doi/10.1002/anie.202421942 by University Of Science, Wiley Online Library on [27/03/2025]. See the Terms and Conditions (https://onlinelibrary.wiley.com/terms-and-conditions) on Wiley Online Library for rules of use; OA articles are governed by the applicable Creative Commons License